Effective Liquid-Phase Exfoliation and Sodium Ion Battery Application of MoS$_2$ Nanosheets

Gyeong Sook Bang,[†,§] Kwan Woo Nam,[‡,§] Jong Yun Kim,[†] Jongwoo Shin,[†] Jang Wook Choi,[‡,*] and Sung-Yool Choi[†,*]

[†]Department of Electrical Engineering and Graphene Research Center, Korea Advanced Institute of Science and Technology (KAIST), Daejeon 305-701, Republic of Korea

[‡]Graduate School of Energy, Environment, Water, and Sustainability (EEWS) and Center for Nature-inspired Technology (CNiT), KAIST Institute NanoCentury, Korea Advanced Institute of Science and Technology (KAIST), Daejeon 305-701, Republic of Korea

Ⓢ Supporting Information

ABSTRACT: Two-dimensional (2D) molybdenum disulfide (MoS$_2$) has been taken much attention for various applications, such as catalyst, energy storage, and electronics. However, the lack of effective exfoliation methods for obtaining 2D materials in a large quantity has been one of the technical barriers for the real applications. We report a facile liquid-phase exfoliation method to improve the exfoliation efficiency for single-layer MoS$_2$ sheets in 1-methyl-2-pyrrolidinone (NMP) with a sodium hydroxide (NaOH) assistant. The concentration of the exfoliated MoS$_2$ nanosheets was greatly improved compared to that achieved with conventional liquid-phase exfoliation methods using NMP solvent. We demonstrate stable operation of sodium-ion battery by using the exfoliated MoS$_2$ and MoS$_2$-rGO composite as anode materials.

KEYWORDS: nanosheets, MoS$_2$, sodium-ion battery, liquid-phase exfoliation, layered materials

Exfoliated MoS$_2$- nanosheet
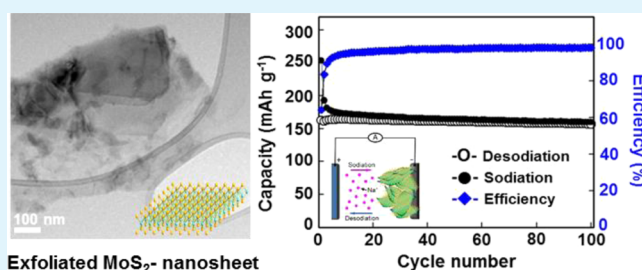
■ INTRODUCTION

Two-dimensional (2D) layered nanomaterials have been taken a great deal of attention for new access to low-dimensional systems.[1−5] Transition metal dichalcongenides (i.e., MX$_2$ (M = Mo, W; X = S, Se, Te)) belong to the family of layered materials, whose crystal structures are built up of covalently bonded X-M-X single-layers that interact by van der Waals forces as graphite.[6] Each single layer consists of two X atom layers and a layer of metal atoms sandwiched between two layers of chalcogens. Previous studies revealed that MX$_2$ has a band gap of 1.1 eV ∼ 2.0 eV.[5,7,8] In the case of MoS$_2$, there is a transition from an indirect bandgap (1.2 eV) in the bulk to a direct bandgap (1.8 eV) in the single-layer. This has attracted interest in a variety of fields, including energy storage, catalysis, solar cell, sensing, and electronic devices.

MoS$_2$ is a nonvolatile and insoluble compound that presents significant challenges in the preparation of thin films. Some approaches to obtain few-layered MoS$_2$ have been reported. A scotch-tape based micromechanical cleavage technique was used to extract a stable single layer MX$_2$.[9] Liquid exfoliation approaches also have been proposed to produce 2D nanosheets and are among the most effective methods for the mass production of exfoliated MX$_2$ nanosheets.[10−12] Li-intercalation is another useful method for exfoliation. However, this method is very sensitive to environmental conditions and is not easy to carry out in ambient conditions. This method also induces a phase change of pristine MoS$_2$ by Li intercalation.[13] Recently, Coleman et al. reported direct exfoliation of MoS$_2$ sheets with thickness of 3−12 nm in organic solvents through sonication.[10] However, this method also shows low yield and requires long sonication time to improve the concentration.[14] An easy exfoliation method with high efficiency of MoS$_2$ direct-dispersion for large-scale application is thus highly demanded.

Here, we report a facile exfoliation technique to improve the liquid exfoliation efficiency for MoS$_2$ dispersion in NMP with NaOH or LiOH. It is well-known that an ion intercalation reaction occurs in highly anisotropic layered structures having weak interlayer bonding forces. Some researchers have reported easy intercalation of alkali metal ions or alkali metal hydroxide into MX$_2$ or graphite with weak interlayer bonding by van der Waals forces.[15−18] To improve the exfoliation efficiency of MoS$_2$, we performed exfoliation by using NMP as a solvent, which provides sufficiently high dielectric strength for MoS$_2$, and NaOH or LiOH as an intercalator into the layered MoS$_2$.
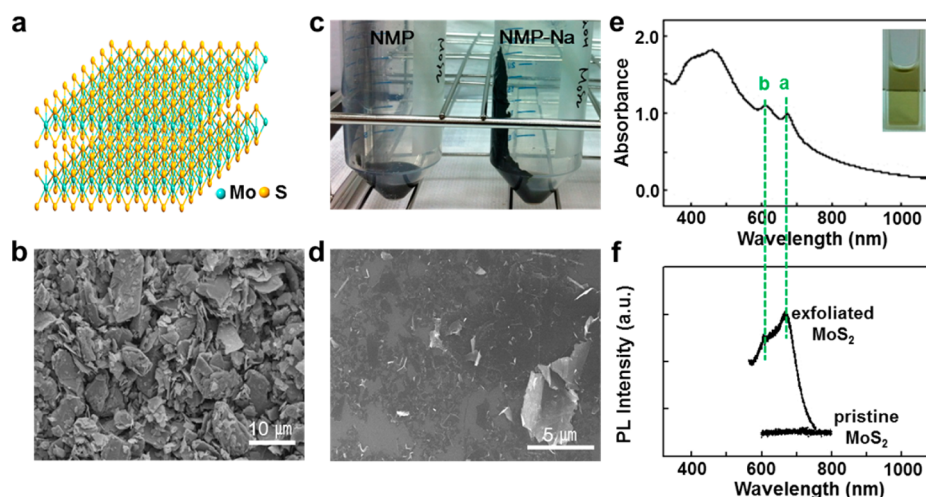
■ EXPERIMENTAL SECTION

Materials. MoS$_2$ powder (<2 μm, 99%, Aldrich) and 1-methyl-2-pyrrolidinone (NMP, 99%, Sigma-Aldrich) were used as received.

Figure 1. (a) The structure of MoS$_2$, (b) SEM images of pristine MoS$_2$ powder, (c) photo image for the effect of exfoliation with NaOH (the right side) and without NaOH (the left side, the control sample), (d) SEM image of the exfoliated MoS$_2$ nanosheets with NaOH in NMP, (e) UV−vis spectrum (inset: photo image of the MoS$_2$ dispersion), and (f) photoluminescence spectrum.

Dispersion of MoS$_2$ Sheets. The dispersions of MoS$_2$ nanosheets were prepared by direct exfoliation with NaOH through sonication in NMP, a commonly used solvent. We prepared the dispersions with various MoS$_2$ concentrations from 1 to 50 mg/mL in 20 mL NMP and NaOH (0.25 mg/mL). The mixture was sonicated for 2 h in a bath sonicator (JAC Ultrasonic 2010, 40 kHz, 200W) with a cooling system to prevent overheating during sonication. For the control test, the MoS$_2$ dispersion was prepared by sonication without NaOH under the same conditions. After the sonication, the exfoliated solution with or without NaOH was centrifuged at 2000 rpm for 30 min using a centrifuge (Hanil Industrial Co., Ltd., Combi 514R) and the sediment was discarded to remove the unexfoliated MoS$_2$ or thick flakes. The exfoliated MoS$_2$ film using of a third solution of the supernatant was prepared to analyze interlayer spacing of MoS$_2$ layers by vacuum filtration using an anodic aluminum oxide (AAO) filter (Anodisc 47, 0.025 μm pores, Whatman) and washed several times with NMP to remove free NaOH and dried in vacuum condition at room temperature for 27 h. (Supporting Information (SI) Figures S1 and S4 XRD of the films) The remained supernatant with or without NaOH was centrifuged at 9000 rpm for 45 min. The supernatant was discarded and fresh NMP was added. The solution was sonicated for 3 min and was centrifuged at 9000 rpm for 45 min to remove most of the free NaOH. This washing process was repeated several times to obtain clean solution without free NaOH. The removal of NaOH was estimated by the pH check of the supernatant using pH test paper after each centrifugation (pH 14 of blue color for sample without washing, pH 6−7 of yellow color for washing sample, SI Figure S1). The final MoS$_2$ dispersions were prepared by redispersion using further sonication for 40 min (SI Figure S1). The resulting solution of between 2000 and 9000 rpm was dark green color and stable for a few days without aggregation. And we also prepared the dispersions with different alkali metal hydroxides in NMP containing 1 mg/mL of MoS$_2$ and 0.25 mg/mL of MOH (M = Li, Na, K).

Characterization. UV−vis spectra of the MoS$_2$ dispersion were recorded using Scinco S-3100 Photodiode array UV−vis spectrophotometer. A quartz cell with a path length of 1.0 cm was used for absorbance. SEM images were obtained using a Sirion FEI scanning electron microscopy (SEM). Raman and photoluminescence (PL) spectra were obtained at 514 nm with a high resolution dispersive Raman spectroscopy (Horiba Jobin Yvon, ARAMIS). X-ray diffraction patterns were collected using a high power microarea X-ray diffractometer (XRD, Rigaku, D/MAX-2500) using Cu Kα radiation. TEM images were taken with a JEOL JEM 2100F transmission electron microscope (TEM). XPS elemental analysis was conducted using a PHI Versaprobe X-ray photoelectron spectroscopy (XPS). The XPS spectrum for S 2p was fitted using a Gaussian−Lorentzian peak

shape after baseline correction. AFM measurements were performed with a Digital Instruments Dimension (D3100, Veeco) and Advanced Scanning Probe Microscope (XE-100, psia). Electrochemical measurements were carried by preparing CR2032 coin-type half-cells in an argon-filled glovebox. Sodium disks served as counter and reference electrodes, and polypropylene films (Celgard-2400) were used as separators. The electrolyte was 1.0 M sodium perchlorate (NaClO$_4$) dissolved in a mixture of fluorinated ethylene carbonate/propylene carbonate (FEC/PC). The working electrodes were fabricated on aluminum foil current collectors by the doctor blading technique. The slurry consisted of 60 wt % active material, 20 wt % acetylene black, and 20 wt % poly(acrylic acid) (PAA) binder. The prepared electrodes were aged for 6 h before any electrochemical processes to ensure good soaking of the electrolyte into the separators and electrodes. Galvanostatic charge/discharge cycling was conducted using a battery tester (WBCS3000L, WonATech, Korea) in the voltage range of 0.4−2.6 V (vs Na|Na$^+$) at 25 °C.

■ RESULT AND DISCUSSION

The dispersions of MoS$_2$ nanosheets were prepared by direct exfoliation of bulk MoS$_2$ powder with NaOH through sonication in NMP. Parts a and b of Figure 1 show the crystal structure of MoS$_2$ and SEM images of pristine MoS$_2$ powder. After exfoliation, the volume of final sediment with the addition of NaOH was much larger than that without the addition of NaOH (Figure 1c).

To attain the quantitative concentration of the dispersion, we prepared the dispersions with various mass concentrations from 1 to 50 mg/mL in 20 mL NMP. The dispersions were obtained from sonication for 2 h and centrifugation at 2000 rpm, and their optical absorbance measurements were obtained. From the absorbance obtained by background subtraction using extrapolation of high wavelength, the concentration of the dispersion were determined using Beer−Lambert law ($A/l = \varepsilon C$),[10] from which the absorption coefficient (ε) was determined. After filtration and drying, we carefully measured the weight of the samples. In a straight line fit between the dispersion mass concentration and the absorbance per unit path length, the slope gives an absorption coefficient at 670 nm of ε = 95.70 mL mg^{-1} m^{-1}. (SI Figure S2) The absorption spectra of the dispersion with different starting mass concentrations from 1 to 50 mg/mL were also obtained. The mass concentration of the dispersion turned out to be 0.6 mg/mL
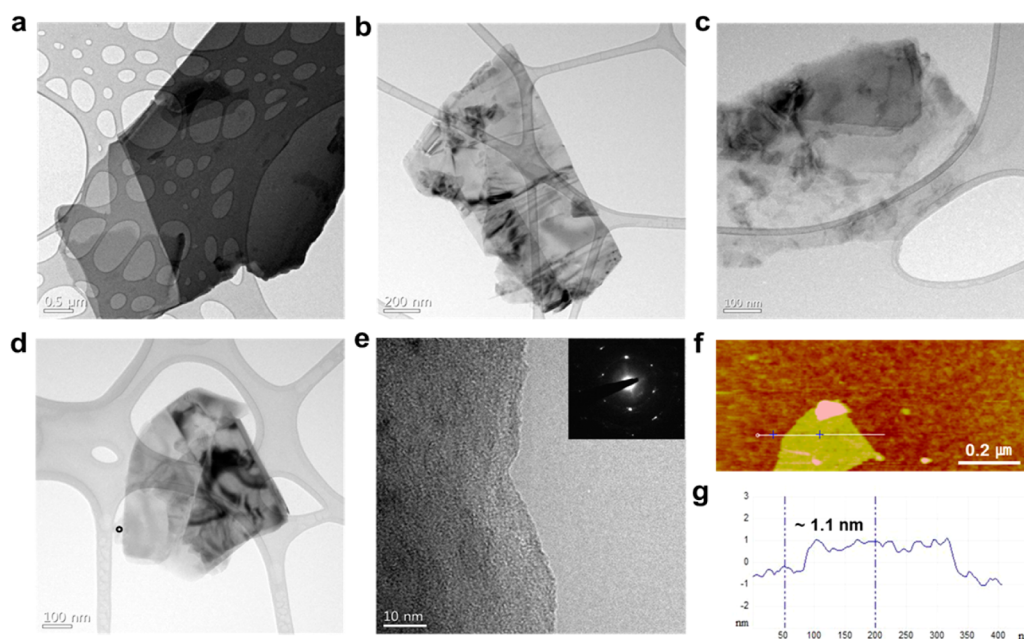
Figure 2. TEM images of (a−d) few-layer MoS$_2$ nanosheets, (e) HRTEM image and electron diffraction pattern in inset at the upper right corner. (f) Tapping-mode AFM image and (g) the corresponding line scan of the MoS$_2$-nanosheet film on SiO$_2$/Si substrate.

for the starting mass concentration of 1 mg/mL. The mass concentration of the dispersion increased linearly (R^2 = 0.99) with increasing the starting mass concentration. The slope of the straight line fit for the MoS$_2$ dispersion gives the yield about 65% by the assistance of NaOH in NMP. (SI Figure S3) The yield is apparently higher than the value in the absence of NaOH (shown in Figure 1c and SI Figure S6) as well as those reported in the literature, such as bare organic solvent only (2.4%)[14] and aqueous dispersion containing surfactant (∼10%).[26] Hence, it can be concluded that the addition of NaOH is very effective for MoS$_2$ exfoliation.

The final MoS$_2$ dispersions were prepared by redispersion of the final sediment using further sonication for 40 min. The SEM image of the final sample film on SiO$_2$/Si clearly shows 2D flakes with basal plane and edges (Figure 1d). Figure 1e is the UV−vis absorption spectrum for the final dispersion at room temperature. The reported data for MoS$_2$ bulk powder were used as a reference.[20] The absorption spectrum of the MoS$_2$ dispersion obtained by our method reveals two peaks (a and b) between 600 and 700 nm and a broad band at around 450 nm with a shoulder at 399 nm. The a and b peaks can be assigned to the characteristics of a 2H-MoS$_2$ nanosheet and correspond to the smallest direct transition.[21] The peak positions for a and b excitons are at 670 nm (1.85 eV) and 607 nm (2.04 eV) with energy separation of 0.19 eV.[6] The values of excitons showed a blue shift compared to the reported data for the bulk powder (748 nm (1.66 eV)).[22] The blue shift is due to the quantum-size confinement. The PL spectrum displays a clear main emission peak at 665 nm and a shoulder peak at 612 nm (Figure 1f). These results are in good agreement with MoS$_2$ thin layers obtained from a liquid-based exfoliation method.[10,12]

We investigated the dispersion of the MoS$_2$ nanosheets via a TEM analysis. Figure 2 shows TEM images of few layer MoS$_2$ nanosheets on a holey carbon TEM grid. TEM images of the MoS$_2$ nanosheets generally show wrinkled sheets that are partially folded. The HRTEM image (Figure 2e) of the MoS$_2$ nanosheet with well-defined edges was taken from the positions

marked by the black circle on the sheet, shown in the left lower side of Figure 2d. The inset of Figure 2e is a typical electron diffraction pattern of exfoliated MoS$_2$.

AFM images provide further information on the thickness of a single-layer and efficient exfoliation of the MoS$_2$ nanosheet. To obtain the correlation between the morphology and thickness of the nanosheet film, we conducted AFM analysis. Parts f and g of Figure 2 are an AFM image and the step height of a single-layer MoS$_2$ nanosheet on SiO$_2$/Si surface. The step height was observed to be about 1.1 nm. This thickness is fairly consistent with values obtained by other groups for single-layer MoS$_2$ prepared with liquid-based exfoliation.[12] To obtain statistical data of the prepared MoS$_2$ nanosheets, we plotted a histogram of the thickness distribution from AFM images (SI Figure S3). A statistical analysis revealed that the nanosheets have an average thickness ranging between 1 and 9 nm, which correspond to 1−9 layers MoS$_2$.

From TEM and AFM images, the nanosheets showed lateral dimensions ranging from 50 nm to 1 μm in size. The single-layer MoS$_2$ sheets show lateral sizes of less than 300 nm. The amount of MoS$_2$ sheet with 1−3 layer thickness is above 85%.

We performed XPS measurement. In Figure 3a, the Mo 3d peaks are assigned to Mo^{4+} 3d$_{5/2}$ (229.3 eV) and Mo^{4+} 3d$_{3/2}$ (232.6 eV), the expected values for Mo^{4+} in MoS$_2$. The corresponding S 2p peak consists of a single doublet of 2p$_{1/2}$ (163.4 eV) and S 2p$_{3/2}$ (162.3 eV), consistent with the S^{2-} type present in MoS$_2$ (Figure 3b). It shows a small peak at around 236 eV, which corresponds to Mo^{6+} 3d$_{5/2}$ from Mo oxidation.

Raman spectra provide an easy and qualitative characterization of MoS$_2$ nanosheet. Raman spectra for pristine MoS$_2$ powder and the exfoliated MoS$_2$ nanosheets with NaOH treatment on a SiO$_2$/Si substrate are shown in Figure 3d. The typical peak, known as the E$^1_{2g}$ peak, at 385.6 cm^{-1} originates from the vibration of Mo−S in-plane mode, and an A$_{1g}$ peak near 408 cm^{-1} from out-of-plane vibrations is also observed. The spectrum for pristine MoS$_2$ powder shows peaks at 383 and 409 cm^{-1}. The peak difference between E$^1_{2g}$ and A$_{1g}$ was 26 cm^{-1} for pristine MoS$_2$ powder and 22.4 cm^{-1} for our MoS$_2$
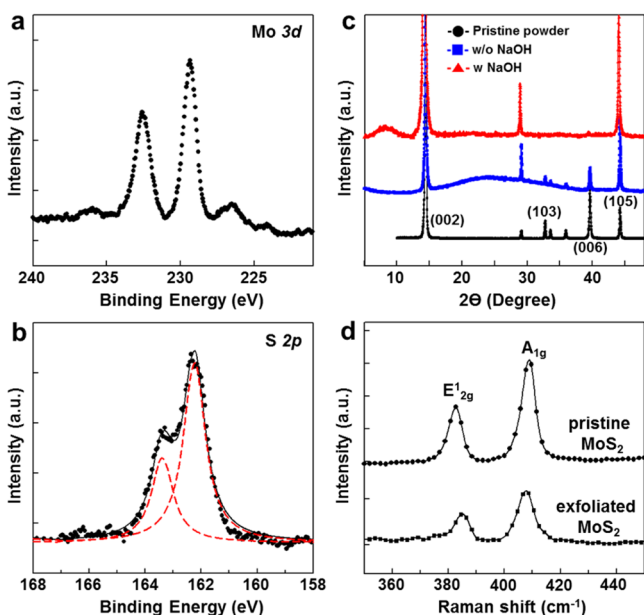
Figure 3. (a) Mo 3d and (b) S 2p xps spectra of the MoS$_2$-nanosheets on SiO$_2$/Si substrate. (c) XRD spectra of the pristine MoS$_2$ powder (indexing JCPDS file No. 00-006-0097) and the MoS$_2$-nanosheets film with (red line) and without (blue line) NaOH treatment. (d) Raman spectra for pristine MoS$_2$ powder and the exfoliated MoS$_2$-nanosheets on SiO$_2$/Si substrate.

dispersion. The peak difference can be used to estimate the number of MoS$_2$ layers and the value of 22.4 cm^{-1} for the prepared MoS$_2$ dispersion corresponds to trilayer MoS$_2$. Furthermore, the line widths (6−7 cm^{-1}) for the MoS$_2$ dispersion are larger than the reported data (2−6 cm^{-1}) of mechanically exfoliated MoS$_2$ single crystals (SI Figure S4).

The line broadening is attributed to a smaller crystallite size and to a greater amount of defects compared to MoS$_2$ single crystals obtained in previous studies[23,24] employing a liquid-based exfoliation method. This is in good agreement with the reported data.[12]

In our exfoliation experiment, NaOH facilitates the exfoliation of MoS$_2$ flakes. To characterize the intercalation of NaOH in the prepared MoS$_2$ nanosheets, we prepared three dispersion samples in the cooling system and attained the corresponding XRD spectra on three restacking films. We compared the results with those of pristine MoS$_2$ powder and an exfoliated MoS$_2$ in NMP without NaOH, as shown in Figure 3c. The XRD spectrum of the pristine powder is assigned by the MoS$_2$ (indexing JCPDS file No. 00-006-0097). The XRD peak of (002) of the restacked MoS$_2$ film in NMP without NaOH presents the same pattern as the (002) peak of pristine MoS$_2$ powder. This suggests that the interlayer spacing of MoS$_2$ was not changed with treatment in NMP, thus indicating that the NMP molecules do not affect intercalation into the interlayer of MoS$_2$. However, the restacked film of MoS$_2$ with NaOH treatment showed the XRD peaks at 2θ = 14.5 ± 0.02° (for (002) peak) and 8.1 ± 0.05°. The peak corresponding to the (002) becomes broadened relative to that of pristine MoS$_2$ powder, and the peak position is similar to that of pristine MoS$_2$ powder. A new peak appeared at a lower diffraction angle than the (002) peak. These results indicate that the interlayer spacing of the film was partially expanded by treatment with NaOH and the crystal structure was not destroyed. The peak broadening might be due to defects and nanometer scale of the

restacked MoS$_2$ sheets. These peak values are similar to those reported for the restacked film by exfoliation of Li-intercalated MoS$_2$ (2θ =14.8° and 7.6°).[12]

To further investigate the dispersibility of MoS$_2$ with other alkali metal hydroxides, we prepared the dispersions in NMP containing LiOH, NaOH, and KOH under conditions of sonication for 2 h and centrifugation at 2000 rpm for 30 min. The MoS$_2$ solutions including alkali metal hydroxides were well dispersed. Their photo images and absorption spectra are shown in SI Figure S6. The resulting dispersions were characterized by UV−vis spectrophotometer. The concentrations of those dispersions were determined by Beer−Lambert law based on the absorbance divided by cell length at 670 nm.[10] The mass concentrations turned out to be 0.80, 0.61, and 0.03 mg/mL for the LiOH, NaOH, and KOH cases, respectively, and 0.03 mg/mL for the bare NMP without any alkali metal hydroxides. Thus, we reach the conclusion that LiOH or NaOH assist increasing exfoliation efficiency significantly while preserving stable dispersion, but KOH was not effective at all. Since the cation radii of alkali metal hydroxides (Li$^+$, Na$^+$, and K$^+$) are 0.076, 0.102, and 0.138 nm, the efficiency of the exfoliation goes higher as the cation size become smaller: LiOH > NaOH > KOH.

With regard to the mechanism of NaOH-assisted exfoliation, layered MX$_2$ or graphite with weak van der Waals forces has been known to allow intercalation of alkali and alkali earth metal hydroxides.[15−19] While substantial in-depth studies are required to grasp detailed mechanism on the intercalation of Na$^+$, an STM study by Shigekawa et al. gave a short clue on the given process.[19] They characterized intercalation of NaOH in highly oriented pyrolytic graphite (HOPG) and MoS$_2$ by engaging STM and charge transfer from the intercalates to HOPG or MoS$_2$. The negatively charged hydroxide ions (OH$^-$) first approach near the Mo atoms with Lewis acid character, during which Na$^+$ ions also approach toward the edges of the MoS$_2$ sheets together. Thus, once Na$^+$ ions reach the edges, the charge transfer seems to play a role as a driving force in facilitating continuous insertion of Na$^+$ ions into the interlayer space in MoS$_2$. (SI Figure S7) Under aggressive stirring, such intercalation of Na$^+$ ions delivers enough energy to break the van der Waals interactions between the layers of MoS$_2$. Therefore, NaOH helps exfoliate the MoS$_2$ layers in NMP, and the exfoliation efficiency of MoS$_2$ nanosheets was greatly improved under sonication.

From the above discussions, we suggest that the improved efficiency of MoS$_2$ exfoliation results from the assisting role of NaOH (or LiOH) in NMP.

Finally, electrochemical properties of the exfoliated MoS$_2$ nanosheets were investigated as an anode material of sodium ion batteries (SIBs). Figure 4a shows charge and discharge curves when measured at a current density of 20 mA g^{-1}. The first sodiation curve exhibits two plateaus, at 0.94 and 0.86 V, while the first desodiation curve exhibits four plateaus, at 1.3, 1.6, 2.3, and 2.5 V. The sodiation and desodiation capacities in the first cycle are 254 and 164 mAh g^{-1}, respectively. These capacities decreased gradually with the repeated cycling and the capacities at the 50th cycle are 165 and 161 mA h g^{-1}, which correspond to a Coulombic efficiency of 97% (Figure 4b). This electrode shows stable cycling behavior for extended cycling period up to 100 cycles (Figure 4b). In fact, the observed initial sodiation capacity is higher sodiation capacity than that of a previous report based on pristine MoS$_2$ powder tested as a SIB active material.[25] In addition, the prepared MoS$_2$ nanosheets
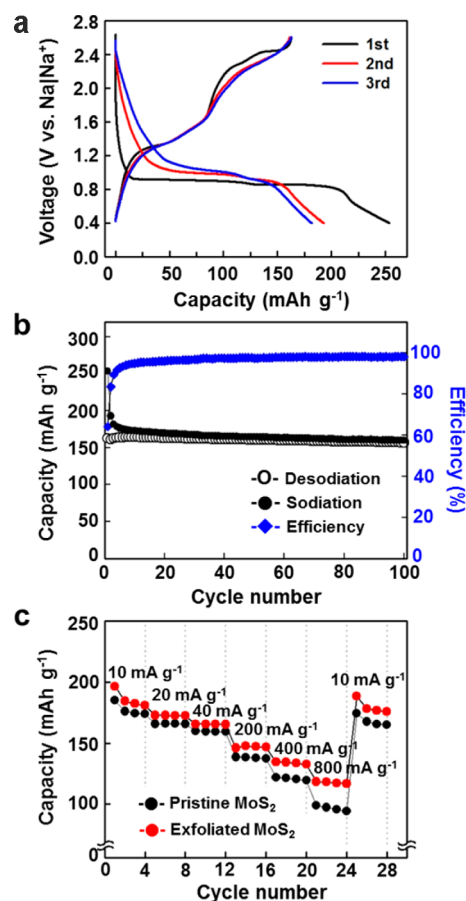
Figure 4. (a) Charge–discharge curves and (b) the cycling performance and their Coulombic efficiencies of the prepared MoS_2 nanosheets. (c) The rate capability of pristine MoS_2 powder (black circle) and the prepared MoS_2 nanosheets (red circle) at various current densities.

exhibit good rate capability and long-term cycling performance (SI Figure S8).

Figure 4c shows the comparative rate capability of the pristine MoS_2 powder and the exfoliated MoS_2 nanosheets at various current densities. At high current densities of 400 and 800 mA g^{-1}, the exfoliated MoS_2 electrode exhibits higher capacities than the pristine MoS_2 electrode, suggesting the improved rate performance of the exfoliated MoS_2 nanosheets based on the decreased diffusion lengths of Na ions. To improve the electrochemical performance further, we prepared a composite electrode containing the exfoliated MoS_2 and reduced graphene oxide (rGO) in a mass ratio of 1:1, and tested its electrochemical performance in the same condition. This composite electrode shows the first discharge capacity of 376 mAh g^{-1}, which is higher than that of the aforementioned pure MoS_2 nanosheets (SI Figure S9) as well as the value reported for MoS_2/graphene composite containing 60 wt % of rGO.[27] Also, the capacity value of the current composite is higher than those (200−240 mAh g^{-1}) of hard carbon materials,[28] which have been the most representative SIB anode materials among various carbon materials.

CONCLUSION

In summary, we report a facile exfoliation technique to improve the liquid exfoliation efficiency for single-layer MoS_2 sheet in NMP with a MOH (M = Li, Na, K) assistant. NMP has been known to have sufficiently high dielectric strength for MoS_2, which may facilitate incorporation of Na+ (or Li+) and OH− into the interplanar spacing of MoS_2. This simple method can be used to prepare single or few-layer nanosheets of MoS_2 with high exfoliation efficiency and good dispersibility. Based on this structural character as well as good dispersion in the given solvent, the exfoliated MoS_2 and MoS_2-rGO composite were identified as competitive anode materials for sodium ion batteries, which are receiving increasing attention for emerging grid-scale energy storage systems due to the availability of low cost raw resources. Finding and optimizing functional SIB anode materials are especially meaningful since no existing materials have warranted the viability as SIB anode materials yet.

ASSOCIATED CONTENT

Supporting Information

Photo image for the pH change after washing the exfoliated MoS_2, absorption spectra for various starting mass concentration and alkali metal hydroxides, AFM analysis of the MoS_2 nanosheets, Raman of MoS_2 single sheet by scotch-tape method, schematic representation for effective exfoliation, cycling performance of the pristine MoS_2 powder and the exfoliated MoS_2, and charge−discharge curve of the MoS_2-rGO (50 wt %) composite electrode. This material is available free of charge via the Internet at http://pubs.acs.org.

AUTHOR INFORMATION

Corresponding Authors
*Fax: +82 42 350 7283. Tel: +82 42 350 7427. Email: sungyool. choi@kaist.ac.kr.
*Email: jangwookchoi@kaist.ac.kr.

Author Contributions
§G.S.B. and K.W.N. contributed equally to this work.

Notes
The authors declare no competing financial interest.

REFERENCES

(1) Geim, A. K.; Novoselov, K. S. The Rise of Graphene. *Nat. Mater.* **2007**, *6*, 183−191.
(2) Novoselov, K. S.; Geim, A. K.; Morozov, S. V.; Jiang, D.; Zhang, Y.; Dubonos, S. V.; Grigorieva, I. V.; Firsov, A. A. Electric Field Effect in Atomically Thin Carbon Films. *Science* **2004**, *306*, 666−669.
(3) Late, D. J.; Liu, B.; Matte, H. S. S. R.; Dravid, V.; Rao, C. N. R. Hysteresis in Single-Layer MoS_2 Field Effect Transistors. *ACS Nano* **2012**, *6*, 5635−5641.
(4) Li, Y.; Wang, H.; Xie, L.; Liang, Y.; Hong, G.; Dai, H. MoS2 Nanoparticles Grown on Graphene: An Advanced Catalyst for the Hydrogen Evolution Reaction. *J. Am. Chem. Soc.* **2011**, *133*, 7296−7299.
(5) Radisavljevic, B.; Radenovic, A.; Brivio, J.; Giacometti, V.; Kis, A. Single-Layer MoS_2 Transistors. *Nat. Nanotechnol.* **2011**, *6*, 147−150.
(6) Benavente, E.; Ana, M. A. S.; Mendizabal, F.; Gonzalez, G. Intercalation Chemistry of Molybdenum Disulfide. *Coord. Chem. Rev.* **2002**, *224*, 87−109.

(7) Mak, K. F.; Lee, C.; Hone, J.; Shan, J.; Heinz, T. F. Atomically Thin MoS_2: A new Direct Gap Semiconductor. *Phys. Rev. Lett.* **2010**, *105*, 136805(4).

(8) Kam, K. K.; Parkinson, B. A. Detailed Photocurrent Spectroscopy of the Semiconducting Group VI Transition Metal Dichalcogenides. *J. Phys. Chem.* **1982**, *86*, 463−467.

(9) Novoselov, K. S.; Jiang, D.; Schedin, F.; Booth, T. J.; Khotkevich, V. V.; Morozov, S. V.; Geim, A. K. Two-Dimensional Atomic Crystals. *Proc. Natl. Acad. Sci. U.S.A.* **2005**, *102*, 10451−10453.

(10) Coleman, J. N.; Lotya, M.; O'Neill, A.; Bergin, S. D.; King, P. J.; Khan, U.; Young, K.; Gaucher, A.; De, S.; Smith, R. J.; Shvets, I. V.; Arora, S. K.; Stanton, G.; Kim, H.-Y.; Lee, K.; Kim, G. T.; Duesberg, G. S.; Hallam, T.; Boland, J. J.; Wang, J. J.; Donegan, J. F.; Grunlan, J. C.; Moriarty, G.; Shmeliov, A.; Nicholls, R. J.; Perkins, J. M.; Grieveson, E. M.; Theuwissen, K.; McComb, D. W.; Nellist, P. D.; Nicolosi, V. Two-Dimensional Nanosheets Produced by Liquid Exfoliation of Layered Materials. *Science* **2011**, *331*, 568−571.

(11) Ramakrishna Matte, H. S. S.; Gomathi, A.; Manna, A. K.; Late, D. J.; Datta, R.; Pati, S. K.; Rao, C. N. R. MoS_2 and WS_2 Analogues of Graphene. *Angew. Chem., Int. Ed.* **2010**, *49*, 4059−4062.

(12) Eda, G.; Yamaguchi, H.; Voiry, D.; Fujita, T.; Chen, M.; Chhowalla, M. Photoluminescence from Chemically Exfoliated MoS_2. *Nano Lett.* **2011**, *11*, 5111−5116.

(13) Heising, J.; Kanatzidis, M. G. Structure of Restacked MoS_2 and WS_2 Elucidated by Electron Crystallography. *J. Am. Chem. Soc.* **1999**, *121*, 638−643.

(14) O'Neill, A.; Khan, U.; Coleman, J. N. Preparation of High Concentration Dispersions of Exfoliated MoS_2 with Increased Flake Size. *Chem. Mater.* **2012**, *24*, 2414−2421.

(15) Somoano, R. B.; Hadek, V.; Rembaum, A. Alkali Metal Intercalates of Molybdenum Disulfide. *J. Chem. Phys.* **1973**, *58*, 697−701.

(16) Gamble, F. R.; Osiecki, J. H.; Cais, M.; Pisharody, R.; DiSalvo, F. J.; Geballe, T. H. Intercalation Complexes of Lewis Bases and Layered Sulfides: A Large Class of New Superconductors. *Science* **1971**, *174*, 493−497.

(17) Rao, G. V. S.; Shafer, M. W.; Tsang, J. C. Intercalation Compounds of Metal Hydroxides with Group V Layered Dichalcogenides. *J. Phys. Chem.* **1975**, *79*, 553−557.

(18) Wei, W.; Wang, J. N. Direct Exfoliation of Graphene in Organic Solvents with Addition of NaOH. *Chem. Commun.* **2011**, *47*, 6888−6890.

(19) Miyake, K.; Shigekawa, H. Surface Structures of Layered Compounds Treated with Alkali-Metal Hydroxide Solutions Studies by Scanning Tunneling Microscopy. *Synth. Met.* **1995**, *71*, 1753−1754.

(20) Remskar, M.; Mrzel, A.; Virsek, M.; Godec, M.; Krause, M.; Kolitsch, A.; Singh, A.; Seabaugh, A. The MoS_2 Nanotubes with Defect-Controlled Electric Properties. *Nanoscale Res. Lett.* **2011**, *6*, 26(6).

(21) Coehoorn, R.; Haas, C.; de Groot, R. A. Electronic Structure of $MoSe_2$, MoS_2, and WSe_2. II. The Nature of the Optical Band Gaps. *Phys. Rev. B* **1987**, *35*, 6203−6206.

(22) Frey, G. L.; Elani, S.; Homyonfer, M.; Feldman, Y.; Tenne, R. Optical-Absorption Spectra of Inorganic Fullerenelike MS_2 (M = Mo, W). *Phys. Rev. B* **1998**, *57*, 6666−6671.

(23) Frey, G. L.; Tenne, R.; Matthews, M. J.; Dresselhaus, M. S.; Dresselhaus, G. Raman and Resonance Raman Investigation of MoS_2 Nanoparticles. *Phys. Rev. B* **1999**, *60*, 2883−2892.

(24) Virsek, M.; Krause, M.; Kolitsch, A.; Mrzel, A.; Iskra, I.; Skapin, S. D.; Remskar, M. The Transformation Pathways of $Mo_6S_2I_8$ Nanowires into Morphology-Selective MoS_2 Nanostructures. *J. Phys. Chem. C* **2010**, *114*, 6458−6463.

(25) Park, J.; Kim, J.-S.; Park, J.-W.; Nam, T.-H.; Kim, K.-W.; Ahn, J.-H.; Wang, G.; Ahn, H.-J. Discharge Mechanism of MoS_2 for Sodium Ion Battery: Electrochemical Measurements and Characterization. *Electrochim. Acta* **2013**, *92*, 427−432.

(26) Smith, R. J.; King, P. J.; Lotya, M.; Wirtz, C.; Khan, U.; De, S.; O'Neill, A.; Duesberg, G. S.; Grunlan, J. C.; Moriarty, G.; Chen, J.; Wang, J.; Minett, A. I.; Nicolosi, V.; Coleman, J. N. Large-Scale Exfoliation of Inorganic Layered Compounds in Aqueous Surfactant Solutions. *Adv. Mater.* **2011**, *23*, 3944−3948.

(27) David, L.; Bhandavat, R.; Singh, G. MoS_2/Graphene Composite Paper for Sodium-Ion Battery Electrodes. *ACS Nano* **2014**, *8*, 1759−1770.

(28) Komaba, S.; Murata, W.; Ishikawa, T.; Yabuuchi, N.; Ozeki, T.; Nakayama, T.; Ogata, A.; Gotoh, K.; Fujiwara, K. Electrochemical Na Insertion and Solid Electrolyte Interphase for Hard-Carbon Electrodes and Application to Na-Ion Batteries. *Adv. Funct. Mater.* **2011**, *21*, 3859−3867.